Author Manuscript

Author Manuscript

Author Manuscript

Author Manuscript

HHS Public Access

Author manuscript

Appl Spectrosc. Author manuscript; available in PMC 2018 February 01.

Published in final edited form as:

Appl Spectrosc. 2017 February ; 71(2): 215–223. doi:10.1177/0003702816654167.

Spatial Mapping of Pyocyanin in *Pseudomonas aeruginosa* Bacterial Communities by Surface Enhanced Raman Scattering

Sneha Polisetti[1,*], **Nameera F. Baig**[2,*], **Nydia Morales-Soto**[3,5], **Joshua D. Shrout**[3,4,5], and **Paul W. Bohn**[1,2,y]

[1]Department of Chemical and Biomolecular Engineering, University of Notre Dame, Notre Dame, IN 46556

[2]Department of Chemistry and Biochemistry, University of Notre Dame, Notre Dame, IN 46556

[3]Department of Civil and Environmental Engineering and Earth Sciences, University of Notre Dame, Notre Dame, IN 46556

[4]Department of Biological Sciences, University of Notre Dame, Notre Dame, IN 46556

[5]Eck Institute for Global Health, University of Notre Dame, Notre Dame, IN 46556

Abstract

Surface Enhanced Raman Spectroscopy (SERS**)** imaging was used in conjunction with Principal Component Analysis (PCA) for the in situ spatiotemporal mapping of the virulence factor pyocyanin, in communities of the pathogenic bacterium *Pseudomonas aeruginosa.* The combination of SERS imaging and PCA analysis provides a robust method for characterization of heterogeneous biological systems while circumventing issues associated with interference from sample autofluorescence and low reproducibility of SERS signals. The production of pyocyanin is found to depend both on the growth carbon source and on the specific strain of *P. aeruginosa* studied. A cystic fibrosis lung isolate strain of *P. aeruginosa* synthesizes and secretes pyocyanin when grown with glucose and glutamate, while the laboratory strain exhibits detectable production of pyocyanin only when grown with glutamate as the source of carbon. Pyocyanin production in the laboratory strain grown with glucose was below the limit of detection of SERS. In addition, the combination of SERS imaging and PCA can elucidate subtle differences in the molecular composition of biofilms. PCA loading plots from the clinical isolate exhibit features corresponding to vibrational bands of carbohydrates, which represent the mucoid biofilm matrix specific to that isolate, features that are not seen in the PCA loading plots of the laboratory strain.

Introduction

Pseudomonas aeruginosa is a Gram-negative bacterium and opportunistic human pathogen that can cause severe chronic infections, leading to a high rate of mortality in patients afflicted with burns, wounds, acute leukemia and cystic fibrosis (CF).[1] The success of *P. aeruginosa* as a pathogen depends partly on the production and secretion of an arsenal of

[y]Corresponding author.

[*]These authors contributed equally to this work

Author Manuscript Author Manuscript Author Manuscript Author Manuscript

virulence factors which include the phenazines – a class of redox-active heterocyclic small-molecule metabolites.[2] Phenazines have also been implicated in several functions critical to the survival of the bacteria, such as biofilm formation and growth. Pyocyanin (5-N-methyl-1-hydroxy-phenazine) is the most widely studied phenazine primarily due to its role in pathogenesis.[3] The presence of pyocyanin in CF lung isolates has been associated with lung damage, which is one of the hallmarks of the disease.[4] High amounts of pyocyanin are typically found in sputum of patients with *P. aeruginosa* infections. It is thought to play an important role in chronic infection - causing progressive loss of lung function, which is the principal cause of death in > 80% of patients.[5]

The pathogenicity of *P. aeruginosa* is strain dependent, with some strains being more virulent than others. For example, between two common laboratory strains, *P. aeruginosa* PA14 is often observed to be more virulent than *P. aeruginosa* PAO1.[6] The nutrients available to the bacteria during growth may also influence phenotypes associated with cell-cell signaling, motility, biofilm formation and the production of virulence factors.[7] *P. aeruginosa* in CF sputum preferentially catabolizes amino acids like L-alanine, L-arginine and L-glutamate over other carbon sources like lactic acid and glucose.[8] Furthermore, aromatic amino acids in the sputum of CF patients may promote synthesis and secretion of the signaling molecule 2-heptyl-3-hydroxy-4-quinolone commonly known as the *Pseudomonas* quinolone signal (PQS). Caldwell *et al.* demonstrated that many CF clinical isolates of *P. aeruginosa* produce more pyocyanin than laboratory strains, like PAO1,[9] and Huang *et al.* showed the effect various carbon sources had on catabolite repression of pyocyanin biosynthesis.[10] Thus, together the phenazines, typified by pyocyanin, and the quinolones/quinolines play important, but still not well understood, roles in mediating the interactions of *P. aeruginosa* with other organisms and its spatial and temporal organization at the community level.[11]

Raman spectroscopy is a non-invasive spectroscopic method capable of yielding detailed molecular information. Importantly, Raman scattering is not affected by the presence of water, making it ideal for the study of biological samples, such as microbial communities, in their natural environment. However, unenhanced Raman signals are inherently weak. They can, however, be greatly amplified by surface enhanced Raman scattering (SERS) which intensifies the signal by factors ranging from 10^6–10^8 (averaged over many molecules) to 10^{14} (special cases of single molecules in metallic nanogaps) when the molecule of interest is in close proximity to an enhancing surface feature.[12] Raman and SERS have both been used for identification and classification of bacterial cells in a variety of samples from single cells to microcolonies.[13–20] Building on this success, Raman microspectroscopy also offers the possibility of studying the microenvironment in bacterial communities and gaining biochemical and spatial information about secreted metabolites and chemical signaling molecules in real time. This capability has to date only been lightly explored, although it is ideally suited to developing an understanding of structure, function and heterogeneity in complex microbial samples, like bacterial biofilms.

In this study we present in situ SERS spatial and temporal mapping of *P. aeruginosa* bacterial communities that show interesting strain- and nutrient-based differences in the production of key chemical signatures, as exemplified by pyocyanin. This study employs

Author Manuscript Author Manuscript Author Manuscript Author Manuscript

SERS imaging of a large area of the sample (25 μm × 25 μm) in contrast to the more common practice of collecting microspectra from a single spot. This large area vibrational spectroscopic mapping provides a more comprehensive picture of the cell-cell relationships in the community, and this is then followed by principal component analysis (PCA) in order to classify the major factors influencing spectral heterogeneity within the community. The combination of SERS and PCA applied to large area data collections produces additional information when compared to averaging single spectra, avoids the random contaminant spectra often seen in SERS, and also provides critical insight into the spatial distribution of metabolites and their role in organizing microbial communities.

Experimental

Materials

Silicon substrates were purchased from WRS Materials (San Jose, CA) as 3-in-diameter wafers of Si (100), then scored and broken into 2 cm × 2 cm tiles before use. Pyocyanin standard, sodium borohydride ($NaBH_4$), and silver nitrate ($AgNO_3$) were purchased from Sigma Aldrich (St. Louis, MO) and used without further purification.

Colloid synthesis

Colloidal silver solutions were prepared according to the standard protocol of Lee and Meisel.[21] A solution of 8.5 mg of $AgNO_3$ in 50 mL water was added dropwise to 150 mL of 1mM $NaBH_4$ while stirring in an ice-bath.[22] The resultant pale yellow solution was stirred and maintained at 4°C for 1 h. UV-visible spectra were used to estimate the size of the nanoparticles. The above method was expected to produce 10–14 nm particles, with the absorbance maxima at 390 nm indicating particles smaller than 12 nm. Samples were then decorated by exposure to a solution containing ~ 3×10^{12} Ag nanoparticles mL^{-1}.

Pellicle biofilm growth and sample preparation

P. aeruginosa strains PAO1C (laboratory strain)[7] and FRD1 (cystic fibrosis lung isolate)[23] were used in this study. Cell cultures were grown overnight at 37°C with shaking at 240 rpm in modified Fastidious Anaerobe Broth (FAB) culture medium[7] supplemented with either 30 mM filter sterilized glucose or glutamate as the source of carbon. Pellicle biofilms (biofilms that form at the air-liquid interface) of FRD1 and PAO1C were grown in a test tube by inoculating 6 mL fresh FAB medium containing 150 μL of 1.2 M glucose or glutamate, with 200 μL of the overnight cell culture (OD=1 at 600 nm) followed by incubation (without shaking) at 37°C until the desired growth time had elapsed.[24] For SERS analysis, 50 μL of the growth at the air-liquid interface was carefully pipetted onto sterile 2 cm × 2 cm silicon wafers, and 100 μL of the colloid solution was then added to the sample and allowed to dry in the dark. The resulting biofilms were physically heterogeneous, with thickness varying with lateral position making it possible to obtain signals from SERS-active sites embedded within the biofilm EPS as well as those at the biofilm-ambient interface. A white light image of a typical transferred biofilm on Si is included as Figure S1.

Author Manuscript Author Manuscript Author Manuscript Author Manuscript

Scanning Electron Microscopy

Dried samples were sputter coated with 2 nm of Au/Ir and scanning electron microscope (SEM) (Magellan 400 FESEM, FEI, Netherlands) images were acquired with a 2.1 mm working distance. The electron beam was operated at an accelerating voltage of 3 kV and a current of 6.3 pA.

Instrumentation and Data Analysis

SERS imaging was performed using a laser scanning confocal Raman microscope (Alpha 300R, WITec, GMBH, Germany), equipped with a 532 nm focused Nd:YAG laser. The laser radiation was delivered to the microscope using a polarization preserving single-mode optical fiber, deflected through a dichroic beam-splitter and focused onto the sample through the microscope objectives. The Raman scattered radiation was collected using the same objectives and delivered through a 50 μm diameter multi-mode fiber to a UHTS 300 spectrometer equipped with a 600 groove mm^{-1} grating and a back-illuminated CCD camera (Newton DU970 N-BV, Andor Inc., cooled to −60°C). SERS images were acquired using a coverslip corrected Nikon water immersion 60× objective (NA=1). Images were obtained by acquiring a full Raman spectrum from each image pixel (80 × 80 pixels or 1600 spectra) over a 25 μm × 25 μm region on the sample with an integration time of 100 ms/spectrum. MATLAB was used to perform Principal Component Analysis (PCA) using previously described custom scripts.[25] The SERS spectra were rendered in IGOR Pro 6.3.

Results and Discussion

The biofilm matrix encases bacterial cells in extracellular polymeric substances (EPS), a complex agglomeration of secreted material that include small molecule metabolites, fluorescent pigments and complex carbohydrates.[26] *Pseudomonas* biofilms produce, among other components, rhamnolipids, quinolines/quinolones, and phenazines,[27] with multiple roles being assigned to each class of compounds, depending on the time and local environment.[28–30]

The first problem to be overcome in the Raman analysis of bacterial communities arises from interference from fluorescent pigments. Fortuitously, as shown in Fig. 1, SERS enables Raman spectral acquisition from highly fluorescent biofilm matrices, presumably because the Ag nanoparticles[31, 32] quench sample autofluorescence, as well as providing the signal enhancements that increase sensitivity compared to unenhanced Raman spectroscopy.[33] Because the Raman signal enhancement in SERS falls off with distance, r, approximately as r^{-10},[34] it requires that the nanoparticles be in close proximity to the analyte molecule.

Scanning electron microscopy (SEM) images of *P. aeruginosa* biofilm samples coated with 10–12 nm diameter Ag colloid were obtained to understand how the nanoparticles were distributed in the sample relative to the cells and the EPS. A representative SEM image in Fig. 2 shows that the nanoparticles are distributed heterogeneously on the sample surface with regions of aggregated clusters interspersed among areas of sparse coverage, which is typical when colloidal particles are used as the enhancing medium.[35, 36] High SERS enhancement is expected from the regions where the clusters are colocalized with the

Author Manuscript Author Manuscript Author Manuscript Author Manuscript

analytes of interest. The spatial length scale is set in bacterial communities and biofilms by the size of *P. aeruginosa* bacterial cells, *i.e.* 1–2 μm. As Fig. 2 illustrates there are relatively few areas this large that are not in contact with Ag colloid.

SERS imaging can also be coupled with multivariate statistical approaches, such as PCA, to provide more detailed insight into the chemical makeup of the EPS. The problem in Raman imaging of extended objects, such as bacterial biofilms, at high spatial resolution with laser scanning confocal Raman microscopy is that a typical volume element (voxel) represents a volume of the order 1 μm^3 while the entire biofilm may occupy a volume 10^8 times larger (1 mm × 1 mm × 100 μm). Thus, it is important to know how to optimally integrate and interpret the spectral data acquired from individual 1 μm^3 voxels. In this context, it is possible to obtain chemical information from principal components that is not available from a single spectrum, or even by averaging spectra collected over different locations, owing to the inherent sample heterogeneity and the need to tradeoff signal-to-noise (S/N) ratio (exacerbated by interference from background and fluorescence) *vs.* acquisition time. This issue is illustrated in Fig. 3 which shows a 25 μm × 25 μm image of the sample generated from the integrated intensities over the 2800 – 3000 cm^{-1} window of the ν(C-H) spectral region. The -CH stretching region is quite strong in the SERS spectra obtained from biofilm EPS. Subsequent PC analysis of the Raman images reveals that the regions where the ν(C-H) is strong are also regions where pyocyanin is present in high abundance and is enhanced relative to other analytes. Three individual spectra from different locations of the image in Fig. 3A are shown in Figs. 3B–D. Clearly, they are all distinctly different from each other. Figs. 3B and C illustrate spectra dominated by unknown sample components, while Fig. 3D contains bands corresponding to pyocyanin, as determined by comparison to the spectrum of pure standard compound.

This heterogeneity in spectral response is a common issue in SERS microscopy. Indeed, heterogeneity arises as a fundamental characteristics of the spatiotemporal production and secretion of extracellular substances, such as pyocyanin. There are a number of different ways that it has been addressed, for example searching for suitable spots that yield “typical” spectra or averaging spectra from multiple locations. Obviously, trying to represent typical spectra is subject to operator bias, while averaging, in addition to being cumbersome and inefficient, can produce misleading results. For example, Fig. 3E shows a spectral response obtained by averaging all 6400 spectra in the image in the area covered by Fig. 3A. The averaging results in improved S/N ratio when compared to single spectra, but it does not resemble any of the individual spectra in Figs. 3B–D, although it does contain the pyocyanin marker band at 1354 cm^{-1} suggesting that pyocyanin is present at comparatively high levels throughout the imaged region. Nevertheless, the fidelity of information transfer from the averaging process is clearly less than ideal.

As an alternative to deterministic data processing approaches, classification approaches based on multivariate statistics show great promise. These approaches have been used extensively in diagnostics, for example bacterial identification from spectral data.[37, 38] Principal component analysis is especially attractive in addressing large multispectral datasets such as those acquired from confocal Raman imaging of heterogeneous biological samples, like bacterial biofilms, where it is important to sample large regions of the

Author Manuscript Author Manuscript Author Manuscript Author Manuscript

sample,[39] and there may be many individual components secreted by the bacteria in the biofilm. This is shown in Fig. 4A, which is the loading plot of the first PC generated from the SERS image in Fig. 4C. The heat map (Fig. 4B) corresponding to PC1 shows that it is localized to a small spot on the sample. This, along with the features in the loading plot, indicates that it may correspond to a contaminant – a valuable conclusion in that it may disregarded so that other principal components can be examined in greater detail.

The second principal component (PC2) has features in the loading plot (Fig. 4D), that resemble Raman bands characteristic of pyocyanin in the sample, and the corresponding heat map (Fig. 4E) shows a relatively homogeneous distribution across the imaged area. Thus, PC2 is chemically relevant to the sample under study. Briefly, this is the strategy we apply to obtain useful information from the sample. The principal component loading plots offer spectral features of much superior quality than averaging of spectra and enable observation of subtle changes in bacterial communities of closely related strains as shown in greater detail below. The PC heat map in Fig. 4E, in particular, indicates that pyocyanin is present in high abundance throughout the imaged region of the biofilm with a small number of isolated regions of extra high intensity.

Having established the utility of mapping the principal components to elucidate behavior in complex multicomponent samples, we next used SERS/PCA mapping to investigate the behavior of two *P. aeruginosa* strains, PAO1C and FRD1, grown using either glucose or glutamate as carbon source. PAO1C pellicle biofilms grown in glucose did not exhibit detectable levels of pyocyanin (data not shown). However, PAO1C grown in glutamate and FRD1 grown in either glucose or glutamate produced detectable levels of pyocyanin (Fig. 5). The first principal components generated from PC analysis of SERS images collected from pellicle biofilms of FRD1 and PAO1C reveal high z-score features at ~1352, 1511, 1572 and 1600 cm^{-1} (Figs. 5A (i), 5B(i), 5C (i)) that are in concordance with vibrational bands representing a combined C-C/C-N stretch and C-H in-plane bend at 1352 cm^{-1}, CH_3 wag and C-H in-plane bend at 1511 cm^{-1} and ring deformation stretch at 1572 and 1600 cm^{-1} [40, 41] present in the SERS spectrum of pyocyanin standard (Figure S2, spectra of medium and background components are given in Figures S3–S6). This suggests that a substantial amount of pyocyanin is secreted by the bacteria within the imaged regions of the biofilm. This point is emphasized by comparing the heat maps of the principal components identified as being dominated by pyocyanin (Figs. 5A(ii), 5B(ii), and 5C(ii)) with the corresponding Raman intensity maps (Figs. 5A(iii), 5B(iii), and 5C(iii)). There is an obvious concordance between the positions of high intensity in the heat maps and in the Raman images, even though the two were selected to examine different features of the biofilm. The Raman images are integrations over the 2800–3000 cm^{-1} region. Full spectra including the 2800–3000 cm^{-1} region are given for regions of high and low intensity for all three samples in Figure S7 and a comparison of Raman images integrated over 600–1800 cm^{-1} and 2800–3000 cm^{-1} are given in Figures S8(a) and S8(b), respectively. Here we use these the Raman images as a proxy for the total density of organic material at a given location, thus suggesting that, at least under these conditions, the portion of the secretome sampled by SERS is dominated by pyocyanin. The predominance of pyocyanin-related features indicates that pycyanin is present in high abundance and is enhanced by AgNPs that are in close proximity within the biofilm EPS.

Author Manuscript Author Manuscript Author Manuscript Author Manuscript

Furthermore, in addition to features corresponding to the vibrational bands of pyocyanin, the most significant principal components from SERS images of FRD1 pellicle biofilms (Figs. 5A(i) and 5B(i)) exhibit a distinct feature at ~ 935 cm^{-1}, that does not appear in the PAO1C biofilm grown on either carbon source. This feature in the loading plot corresponds to vibrational bands associated with C-C-H and C-O-H modes of carbohydrates.[42, 43] The presence of carbohydrates in greater abundance in FRD1 biofilms is associated with the mucoid phenotype characteristic of the FRD1 strain, which is considered to provide protection to the bacteria against the host immune system, phagocytosis and antibiotics,[44] allowing the bacteria to cause persistent infections in the host. Beyond its chemical interpretation, the presence of the 935 cm^{-1} feature and its association with a non-pyocyanin source serves to highlight the fact that principal components are not necessarily derived from a single molecular source and that they must, therefore, be interpreted with care. Finally, the obvious differences in pyocyanin production from FRD1 and PAO1C strains grown on the two carbon sources suggest corresponding differences in the biosynthetic pathways utilized at the sub-species level. Whereas PAO1C is competent to synthesize phenazines (of which pyocyanin is the most abundant member) from glutamate, but not glucose, FRD1, along with other morphological differences in EPS production, is clearly competent to biosynthesize pyocyanin from either carbon source.

Conclusion

SERS imaging produced high quality data from spatially distinct regions of single biofilm samples and across multiple biofilm samples, making it a suitable technique for chemometric analysis. The use of SERS in conjunction with PCA allows rapid sample analysis, eliminating the need to find an optimal location thus bypassing inherent difficulties associated with the analysis of biological samples, such as autofluorescence from cellular metabolites. Studies of bacterial communities, like biofilms, can especially benefit from this approach as it offers similar enhancement factors as engineered SERS substrates fabricated using e-beam or chemical assembly, but uses cost-effective metal nanoparticle colloids, which can be easily synthesized in most laboratory settings. Furthermore, Ag nanoparticle mediated SERS samples were effective in reducing background fluorescence, a particularly important attribute in light of the fluorescent nature of the phenazine class of secreted virulence factors. Finally, we note the special nature of SERS, the media and geometries that are efficient at enhancing Raman scattering, and the potential for biased sampling. Given the highly non-linear nature of SERS hot spots,[45–47] it is at least possible that molecules with a strong propensity to bind to Ag nanoparticles will experience a disproportionate enhancement. This would be an aid in the study of phenazines, but it presents a factor which must be weighed in interpreting the data.

Supplementary Material

Refer to Web version on PubMed Central for supplementary material.

Author Manuscript Author Manuscript Author Manuscript Author Manuscript

Acknowledgments

This work was supported by the National Institute of Allergy and Infectious Disease grant 1R01AI113219-01 (NFB and LM-S) and the Department of Energy through a subaward from Oak Ridge National Laboratory (PTX-UT-Battelle), grant ORNL-4000132808 (SP).

References

1. Hattemer A, Hauser A, Diaz M, Scheetz M, Shah N, Allen JP, Porhomayon J, El-Solh AA. Bacterial and clinical characteristics of health care-and community-acquired bloodstream infections due to Pseudomonas aeruginosa. Antimicrob Agents Chemother. 2013; 57(8):3969–3975. [PubMed: 23733476]
2. Price-Whelan A, Dietrich LEP, Newman DK. Rethinking 'secondary' metabolism: physiological roles for phenazine antibiotics. Nat Chem Biol. 2006; 2(4):221–221.
3. Pierson LS 3rd, Pierson EA. Metabolism and function of phenazines in bacteria: impacts on the behavior of bacteria in the environment and biotechnological processes. Appl Microbiol Biotechnol. 2010; 86(6):1659–1670. [PubMed: 20352425]
4. Lau GW, Hassett DJ, Ran H, Kong F. The role of pyocyanin in Pseudomonas aeruginosa infection. Trends Mol Med. 2004; 10(12):599–606. [PubMed: 15567330]
5. Boucher RC. An overview of the pathogenesis of cystic fibrosis lung disease. Adv Drug Delivery Rev. 2002; 54(11):1359–1371.
6. Mikkelsen H, McMullan R, Filloux A. The Pseudomonas aeruginosa Reference Strain PA14 Displays Increased Virulence Due to a Mutation in ladS. Plos One. 2011; 6(12)
7. Shrout JD, Chopp DL, Just CL, Hentzer M, Givskov M, Parsek MR. The impact of quorum sensing and swarming motility on Pseudomonas aeruginosa biofilm formation is nutritionally conditional. Mol Microbiol. 2006; 62(5):1264–1277. [PubMed: 17059568]
8. Palmer KL, Aye LM, Whiteley M. Nutritional Cues Control Pseudomonas aeruginosa Multicellular Behavior in Cystic Fibrosis Sputum. J Bacteriol. 2009; 191(8):2906–2906.
9. Caldwell CC, Chen Y, Goetzmann HS, Hao YH, Borchers MT, Hassett DJ, Young LR, Mavrodi D, Thomashow L, Lau GW. Pseudomonas aeruginosa Exotoxin Pyocyanin Causes Cystic Fibrosis Airway Pathogenesis. Am J Pathol. 2009; 175(6):2473–2488. [PubMed: 19893030]
10. Huang JF, Sonnleitner E, Ren B, Xu YQ, Haas D. Catabolite Repression Control of Pyocyanin Biosynthesis at an Intersection of Primary and Secondary Metabolism in Pseudomonas aeruginosa. Appl Environ Microbiol. 2012; 78(14):5016–5020. [PubMed: 22562990]
11. Sismaet HJ, Webster TA, Goluch ED. Up-regulating pyocyanin production by amino acid addition for early electrochemical identification of Pseudomonas aeruginosa. Analyst. 2014; 139(17):4241–4246. [PubMed: 24998317]
12. Lombardi JR, Birke RL. A Unified View of Surface-Enhanced Raman Scattering. Acc Chem Res. 2009; 42(6):734–742. [PubMed: 19361212]
13. Jarvis RM, Goodacre R. Discrimination of bacteria using surface-enhanced Raman spectroscopy. Anal Chem. 2004; 76(1):40–47. [PubMed: 14697030]
14. Maquelin K, Choo-Smith LP, Vreeswijk T van, Endtz HP, Smith B, Bennett R, Bruining HA, Puppels GJ. Raman spectroscopic method for identification of clinically relevant microorganisms growing on solid culture medium. Anal Chem. 2000; 72(1):12–19. [PubMed: 10655628]
15. Schuster KC, Urlaub E, Gapes JR. Single-cell analysis of bacteria by Raman microscopy: spectral information on the chemical composition of cells and on the heterogeneity in a culture. J Microbiol Methods. 2000; 42(1):29–38. [PubMed: 11000428]
16. Zhou HB, Yang DT, Ivleva NP, Mircescu NE, Niessner R, Haisch C. SERS Detection of Bacteria in Water by in Situ Coating with Ag Nanoparticles. Anal Chem. 2014; 86(3):1525–1533. [PubMed: 24387044]
17. Halvorson RA, Vikesland PJ. Surface-Enhanced Raman Spectroscopy (SERS) for Environmental Analyses. Environ Sci Technol. 2010; 44(20):7749–7755. [PubMed: 20836559]
18. Jarvis RM, Goodacre R. Characterisation and identification of bacteria using SERS. Chem Soc Rev. 2008; 37(5):931–936. [PubMed: 18443678]

Author Manuscript Author Manuscript Author Manuscript Author Manuscript

19. Porter MD, Lipert RJ, Siperko LM, Wang G, Narayanana R. SERS as a bioassay platform: fundamentals, design, and applications. Chem Soc Rev. 2008; 37(5):1001–1011. [PubMed: 18443685]
20. Tripp RA, Dluhy RA, Zhao YP. Novel nanostructures for SERS biosensing. Nano Today. 2008; 3(3–4):31–37.
21. Lee P, Meisel D. Adsorption and surface-enhanced Raman of dyes on silver and gold sols. J Phys Chem. 1982; 86(17):3391–3395.
22. Podstawka E, Ozaki Y, Proniewicz LM. Part I: Surface-enhanced Raman spectroscopy investigation of amino acids and their homodipeptides adsorbed on colloidal silver. Appl Spectrosc. 2004; 58(5):570–580. [PubMed: 15165334]
23. Ohman DE, Chakrabarty AM. Genetic-Mapping of Chromosomal Determinants for the Production of the Exopolysaccharide Alginate in a Pseudomonas-Aeruginosa Cystic-Fibrosis Isolate. Infect Immun. 1981; 33(1):142–148. [PubMed: 6790439]
24. O'Toole GA, Kolter R. Initiation of biofilm formation in Pseudomonas fluorescens WCS365 proceeds via multiple, convergent signalling pathways: a genetic analysis. Mol Microbiol. 1998; 28(3):449–461. [PubMed: 9632250]
25. Ahlf DR, Masyuko RN, Hummon AB, Bohn PW. Correlated mass spectrometry imaging and confocal Raman microscopy for studies of three-dimensional cell culture sections. Analyst. 2014; 139(18):4578–4585. [PubMed: 25030970]
26. Flemming HC, Neu TR, Wozniak DJ. The EPS matrix: The "House of Biofilm cells". J Bacteriol. 2007; 189(22):7945–7947. [PubMed: 17675377]
27. Perneel M, D'Hondt L, Maeyer K De, Adiobo A, Rabaey K, Hofte M. Phenazines and biosurfactants interact in the biological control of soil-borne diseases caused by Pythium spp. Environ Microbiol. 2008; 10(3):778–788. [PubMed: 18237310]
28. Parsek MR, Greenberg EP. Quorum sensing signals in development of Pseudomonas aeruginosa biofilms. Methods Enzymol. 1999; 310:43–55. [PubMed: 10547781]
29. de Kievit TR. Quorum sensing in Pseudomonas aeruginosa biofilms. Environ Microbiol. 2009; 11(2):279–288. [PubMed: 19196266]
30. Lequette Y, Greenberg EP. Timing and localization of rhamnolipid synthesis gene expression in Pseudomonas aeruginosa biofilms. J Bacteriol. 2005; 187(1):37–44. [PubMed: 15601686]
31. Mihalcea C, Buchel D, Atoda N, Tominaga J. Intrinsic fluorescence and quenching effects in photoactivated reactively sputtered silver oxide layers. J Am Chem Soc. 2001; 123(29):7172–7173. [PubMed: 11459503]
32. Meyer SA, Le Ru EC, Etchegoin PG. Quantifying resonant Raman cross sections with SERS. J Phys Chem A. 2010; 114(17):5515–5519. [PubMed: 20377210]
33. Le Ru EC, Meyer M, Etchegoin PG. Proof of single-molecule sensitivity in surface enhanced Raman scattering (SERS) by means of a two-analyte technique. J Phys Chem B. 2006; 110(4): 1944–1948. [PubMed: 16471765]
34. Kennedy BJ, Spaeth S, Dickey M, Carron KT. Determination of the distance dependence and experimental effects for modified SERS substrates based on self-assembled monolayers formed using alkanethiols. J Phys Chem B. 1999; 103(18):3640–3646.
35. Kahraman M, Zamaleeva AI, Fakhrullin RF, Culha M. Layer-by-layer coating of bacteria with noble metal nanoparticles for surface-enhanced Raman scattering. Anal Bioanal Chem. 2009; 395(8):2559–2567. [PubMed: 19795108]
36. Moskovits M. Surface-enhanced Raman spectroscopy: a brief retrospective. J Raman Spectrosc. 2005; 36(6–7):485–496.
37. Xu LJ, Lei ZC, Li JX, Zong C, Yang CJ, Ren B. Label-Free Surface-Enhanced Raman Spectroscopy Detection of DNA with Single-Base Sensitivity. J Am Chem Soc. 2015; 137(15): 5149–5154. [PubMed: 25835155]
38. Driskell JD, Zhu Y, Kirkwood CD, Zhao YP, Dluhy RA, Tripp RA. Rapid and Sensitive Detection of Rotavirus Molecular Signatures Using Surface Enhanced Raman Spectroscopy. PLos One. 2010; 5(4)
39. Mobili P, Londero A, De Antoni G, Gomez-Zavaglia A, Araujo-Andrade C, Avila-Donoso H, Ivanov-Tzonchev R, Moreno I, Frausto-Reyes C. Multivariate analysis of Raman spectra applied

Author Manuscript Author Manuscript Author Manuscript Author Manuscript

to microbiology Discrimination of microorganisms at the species level. Rev Mex Fis. 2010; 56(5): 378–385.

40. Wu XM, Chen J, Li XB, Zhao YP, Zughaier SM. Culture-free diagnostics of Pseudomonas aeruginosa infection by silver nanorod array based SERS from clinical sputum samples. Nanomed Nanotechnol Biol Med. 2014; 10(8):1863–1870.
41. Jeong DH, Suh JS, Moskovits M. Photochemical reactions of phenazine and acridine adsorbed on silver colloid surfaces. J Phys Chem B. 2000; 104(31):7462–7467.
42. Campos-Vallette MM, Chandia NP, Clavijo E, Leal D, Matsuhiro B, Osorio-Roman IO, Torres S. Characterization of sodium alginate and its block fractions by surface-enhanced Raman spectroscopy. J Raman Spectrosc. 2010; 41(7):758–763.
43. Schmid T, Messmer A, Yeo BS, Zhang WH, Zenobi R. Towards chemical analysis of nanostructures in biofilms II: tip-enhanced Raman spectroscopy of alginates. Anal Bioanal Chem. 2008; 391(5):1907–1916. [PubMed: 18427785]
44. Pritt B, O'Brien L, Winn W. Mucoid Pseudomonas in cystic fibrosis. Am J Clin Pathol. 2007; 128(1):32–34. [PubMed: 17580270]
45. Camden JP, Dieringer JA, Wang Y, Masiello DJ, Marks LD, Schatz GC, Van Duyne RP. Probing the structure of single-molecule surface-enhanced Raman scattering hot spots. J Am Chem Soc. 2008; 130(38):12616. [PubMed: 18761451]
46. Kneipp K, Kneipp H, Dresselhaus MS, Lefrant S. Surface-enhanced Raman scattering on single-wall carbon nanotubes. Philos Trans R Soc London, Ser A. 2004; 362(1824):2361–2373.
47. Wustholz KL, Henry A-I, McMahon JM, Freeman RG, Valley N, Piotti ME, Natan MJ, Schatz GC, Van Duyne RP. Structure-Activity Relationships in Gold Nanoparticle Dimers and Trimers for Surface-Enhanced Raman Spectroscopy. J Am Chem Soc. 2010; 132(31):10903–10910. [PubMed: 20681724]

Author Manuscript Author Manuscript Author Manuscript Author Manuscript

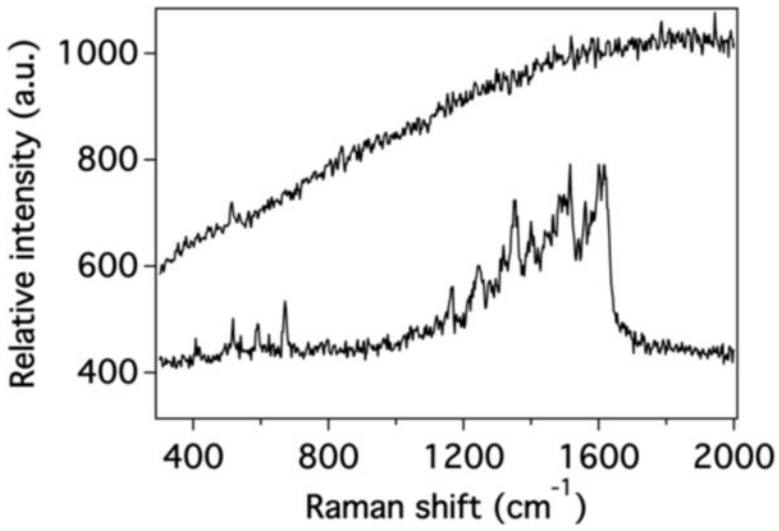

Figure 1.

Comparison of spectra generated from a *P. aeruginosa* bacterial community under normal Raman conditions (*top*) and with the addition of ~12 nm Ag colloid to generate SERS (*bottom*). Raman and autofluorescence spectra have been scaled differently to appear on the same plot.

Author Manuscript Author Manuscript Author Manuscript Author Manuscript

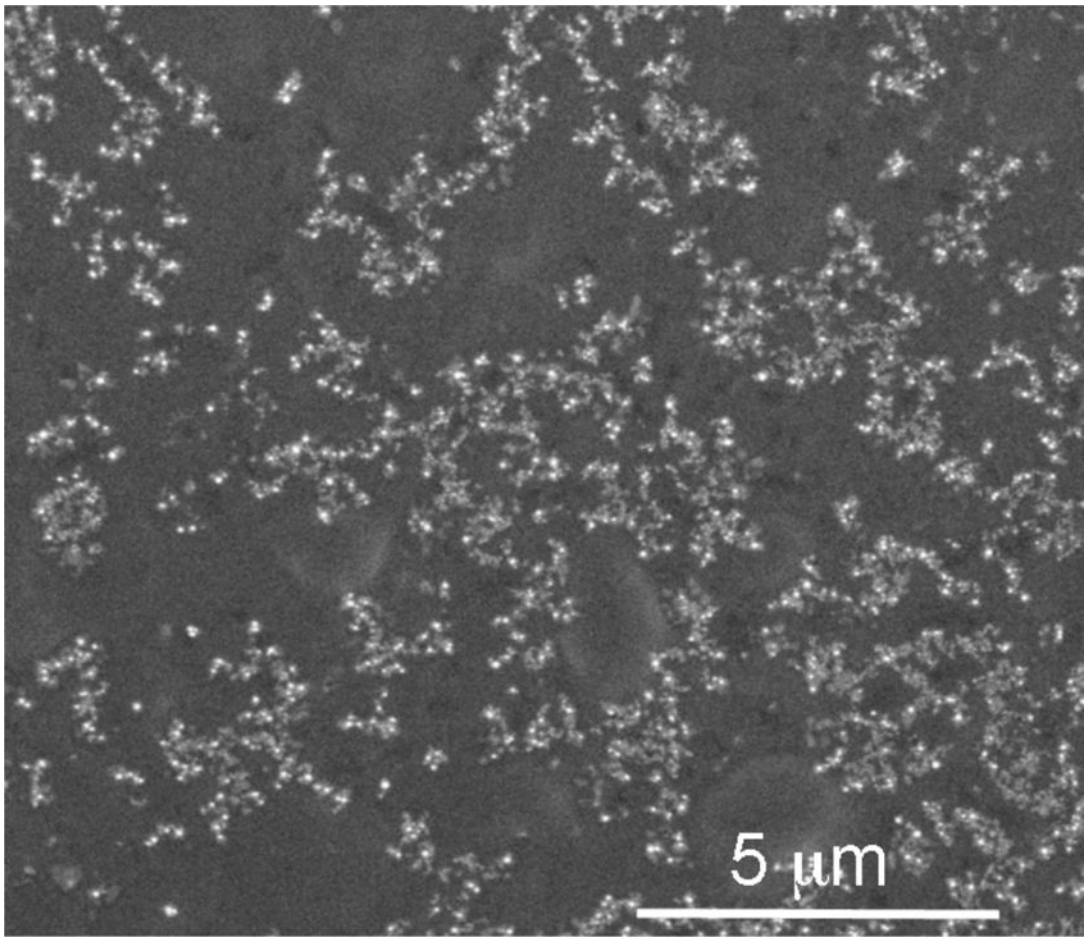

Figure 2.
SEM image taken from a representative region of a 24 h FRD1 pellicle biofilm grown in glucose and decorated with 12 nm Ag nanoparticles showing the spatial distribution and state of aggregation of Ag nanoparticles.

Author Manuscript Author Manuscript Author Manuscript Author Manuscript

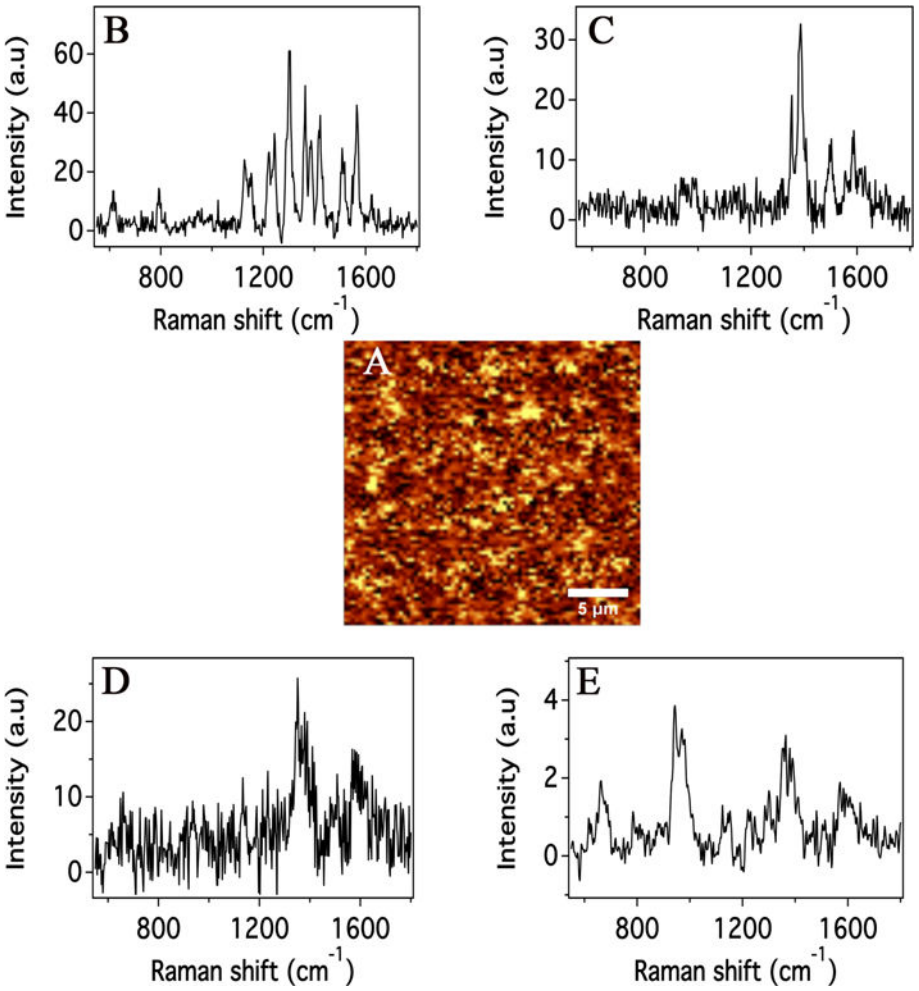

Figure 3.

(A) SERS image constructed as a heat map of the integrated intensity in the range 2800–3000 cm^{-1}, generated from a 48 h FRD1 pellicle biofilm grown in glucose. **(B)**, **(C)** and **(D)** SERS spectra of individual voxels obtained from different spatial locations in the image displayed in **A**. **(E)** SERS spectrum obtained by averaging all of the spectra obtained within the image in **(A)**, *i.e.* the spatially-averaged spectrum.

Author Manuscript Author Manuscript Author Manuscript Author Manuscript

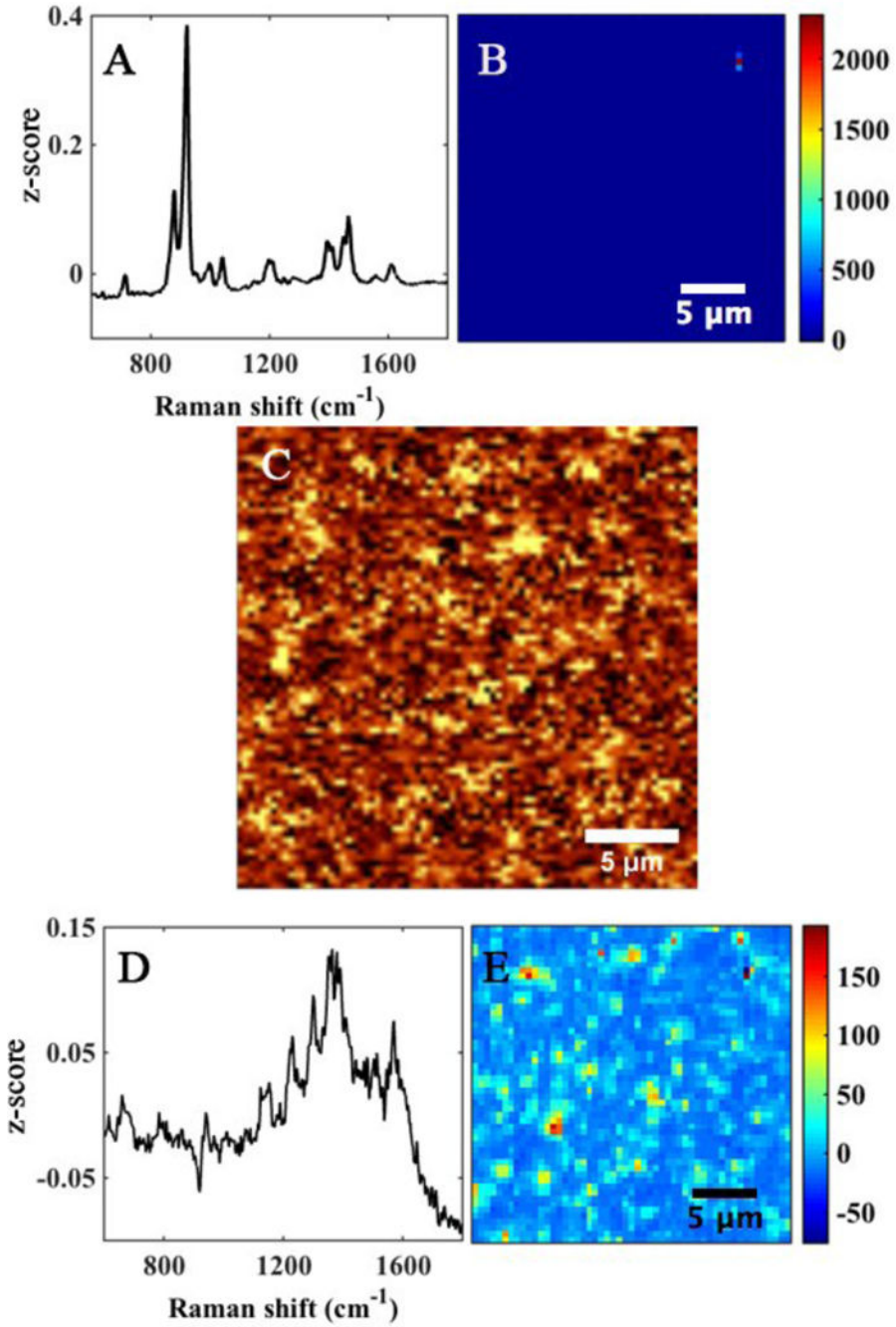

Figure 4.

SERS imaging and PC analysis of a representative area of a 48 h FRD1 pellicle biofilm. (**A**) and (**D**) are loading plots of PC1 and PC2 generated from the SERS image **(C)** which is integrated over the 2800–3000 cm^{-1} filter; (**B**) and (**E**) are heat maps of PC1 and PC2, respectively.

Author Manuscript Author Manuscript Author Manuscript Author Manuscript

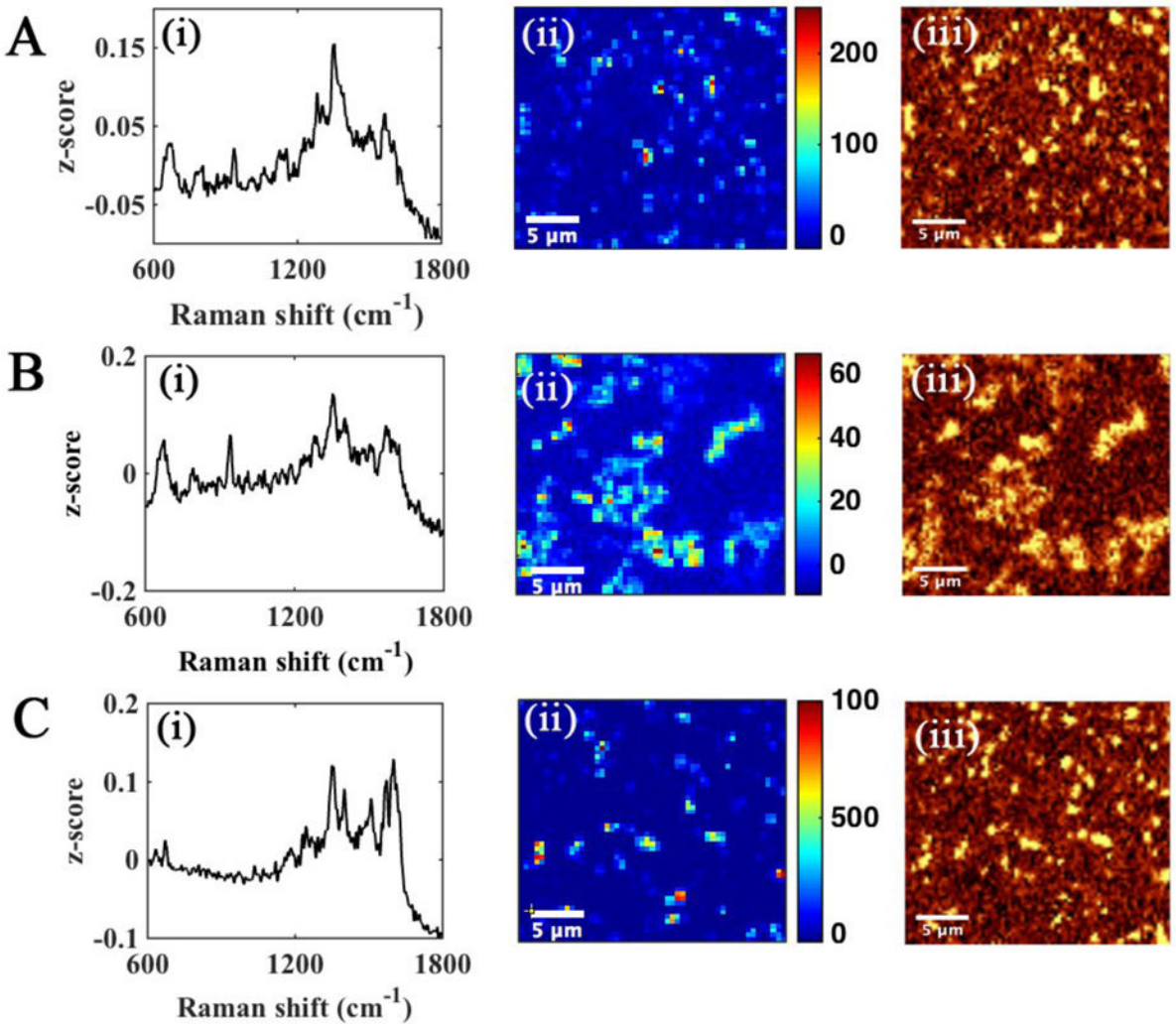

Figure 5.

Analysis of 24 h pellicle biofilms of *P. aeruginosa* FRD1 and PAO1C strains in response to the source of carbon. Raman spectral loadings (i), principal component heat maps (ii), and SERS images (iii) integrated over 2800–3000 cm^{-1} for representative regions of pellicle biofilms derived from *P. aeruginosa* FRD1 (A–B) and PAO1C (C) are shown. Glucose (A and C) and glutamate (B) were provided as carbon sources.

SUPPLEMENTARY MATERIAL

Spatial Mapping of Pyocyanin in *Pseudomonas aeruginosa* Bacterial Communities by Surface Enhanced Raman Scattering

Sneha Polisetti[1*], Nameera F. Baig[2*], Nydia Morales-Soto[3,5], Joshua D. Shrout[3,4,5], and Paul W. Bohn[1,2y^]

[1]Department of Chemical and Biomolecular Engineering, University of Notre Dame, Notre Dame, IN 46556

[2]Department of Chemistry and Biochemistry, University of Notre Dame, Notre Dame, IN 46556

[3]Department of Civil and Environmental Engineering and Earth Sciences, University of Notre Dame, Notre Dame, IN 46556

[4]Department of Biological Sciences, University of Notre Dame, Notre Dame, IN 46556

[5]Eck Institute for Global Health, University of Notre Dame, Notre Dame, IN 46556

*These authors contributed equally to this work

[y^]Corresponding author

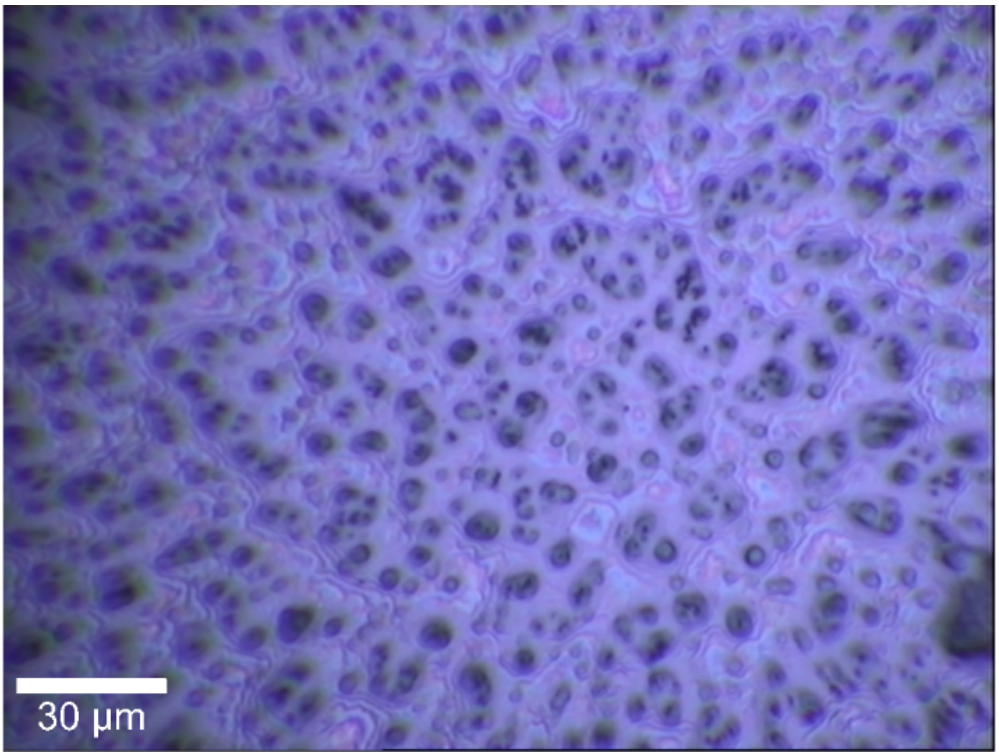

Figure S1. White light reflectance image of transferred biofilm on Si wafer, acquired at 40x magnification, showing large scale structure.

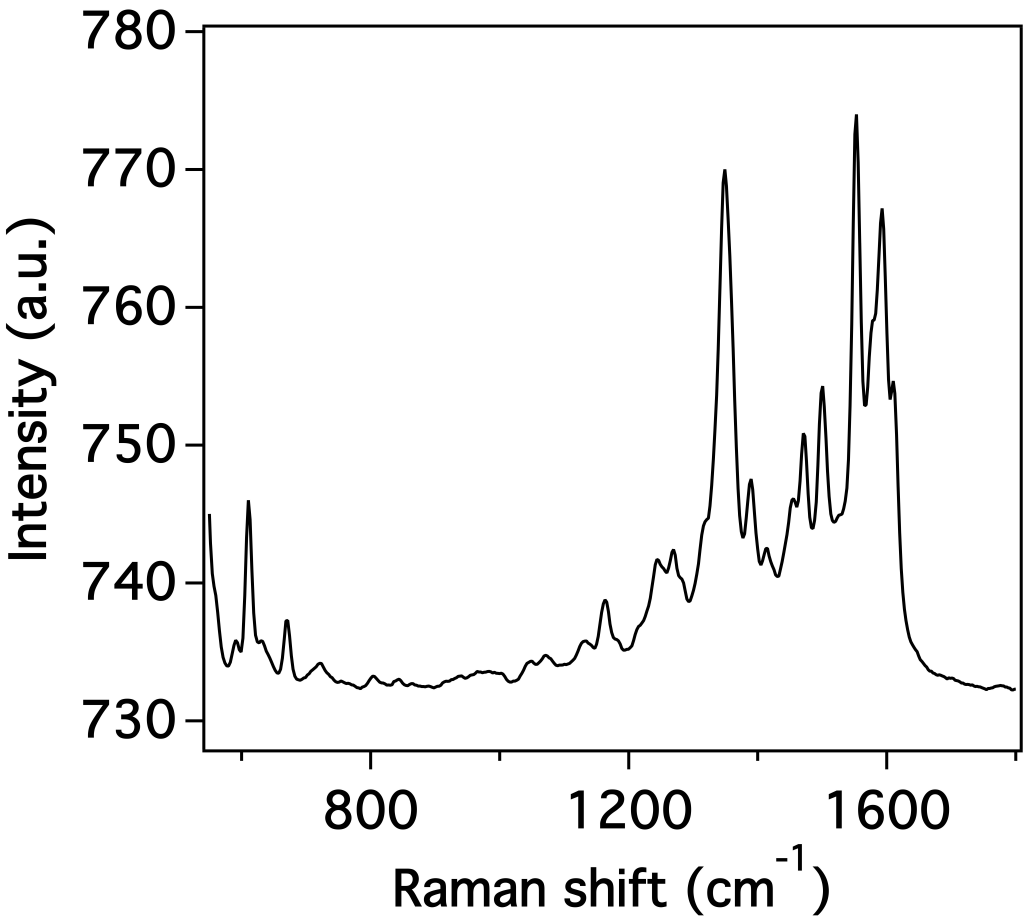

Figure S2. SERS spectrum (average of 6400 spectra collected over 25 μm x 25 μm area *i.e.* the spatially-averaged spectrum) of pyocyanin standard.

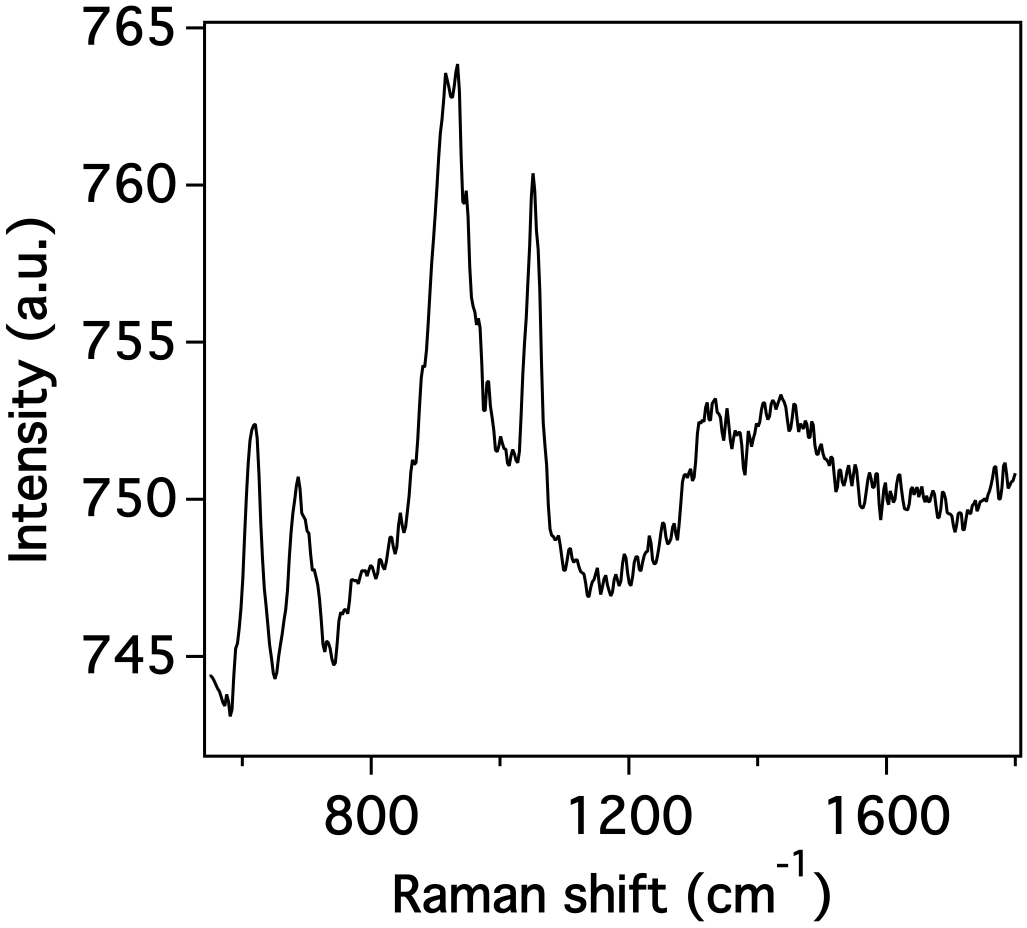

Figure S3. Raman spectrum (spatially-averaged) of Ag colloid (control experiment).

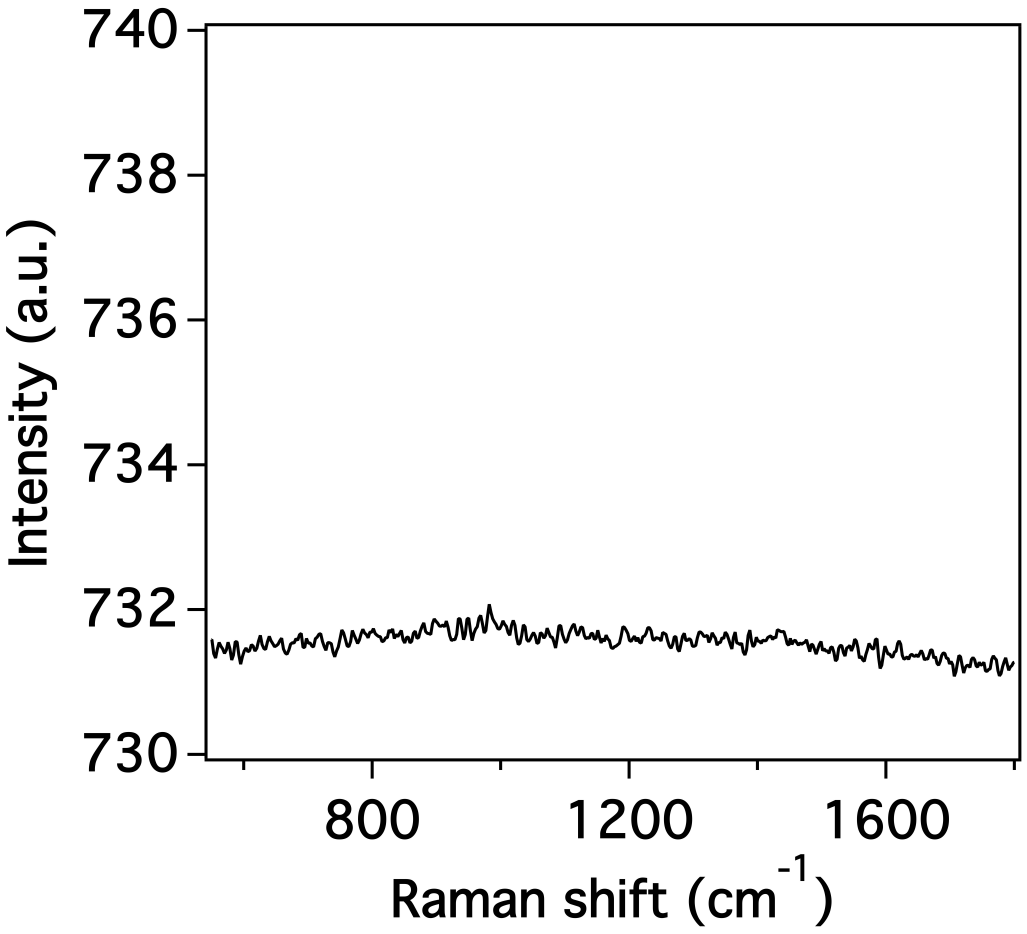

Figure S4. SERS spectrum (spatially-averaged) of FAB + glucose growth media with Ag colloid (control experiment).

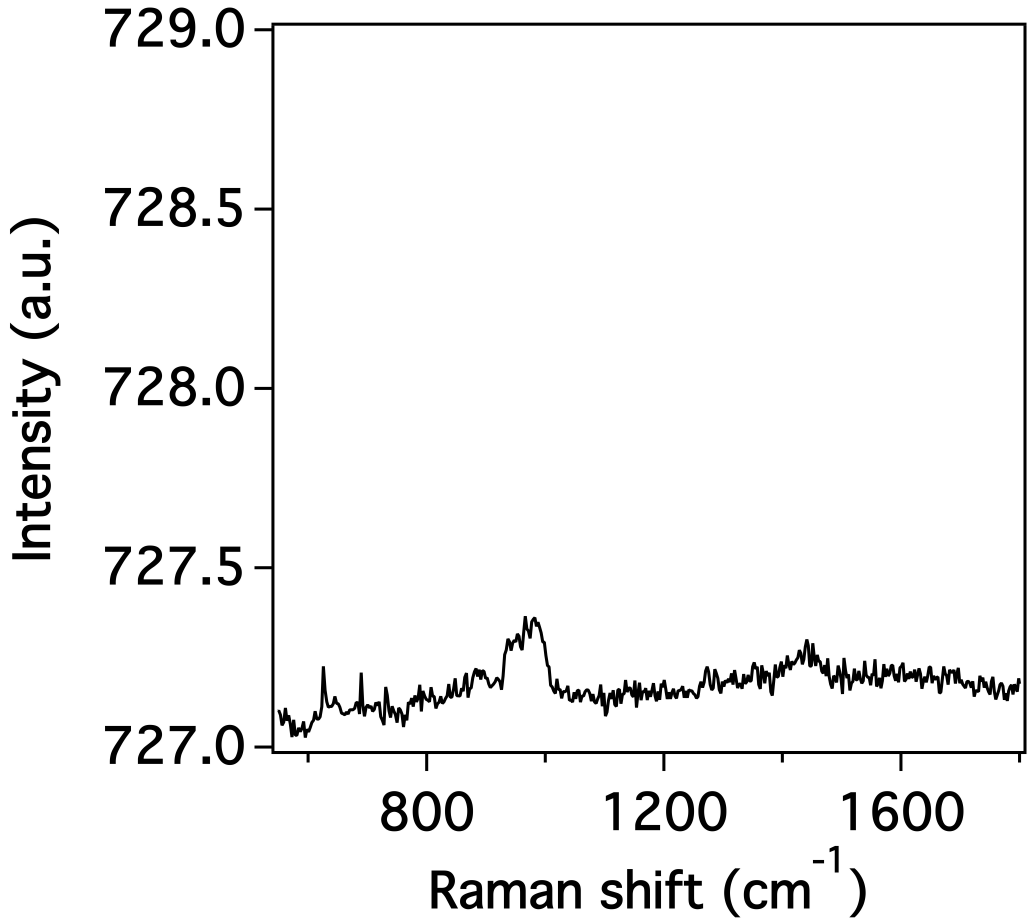

Figure S5. SERS spectrum (spatially-averaged) of FAB + glutamate growth media with Ag colloid (control experiment).

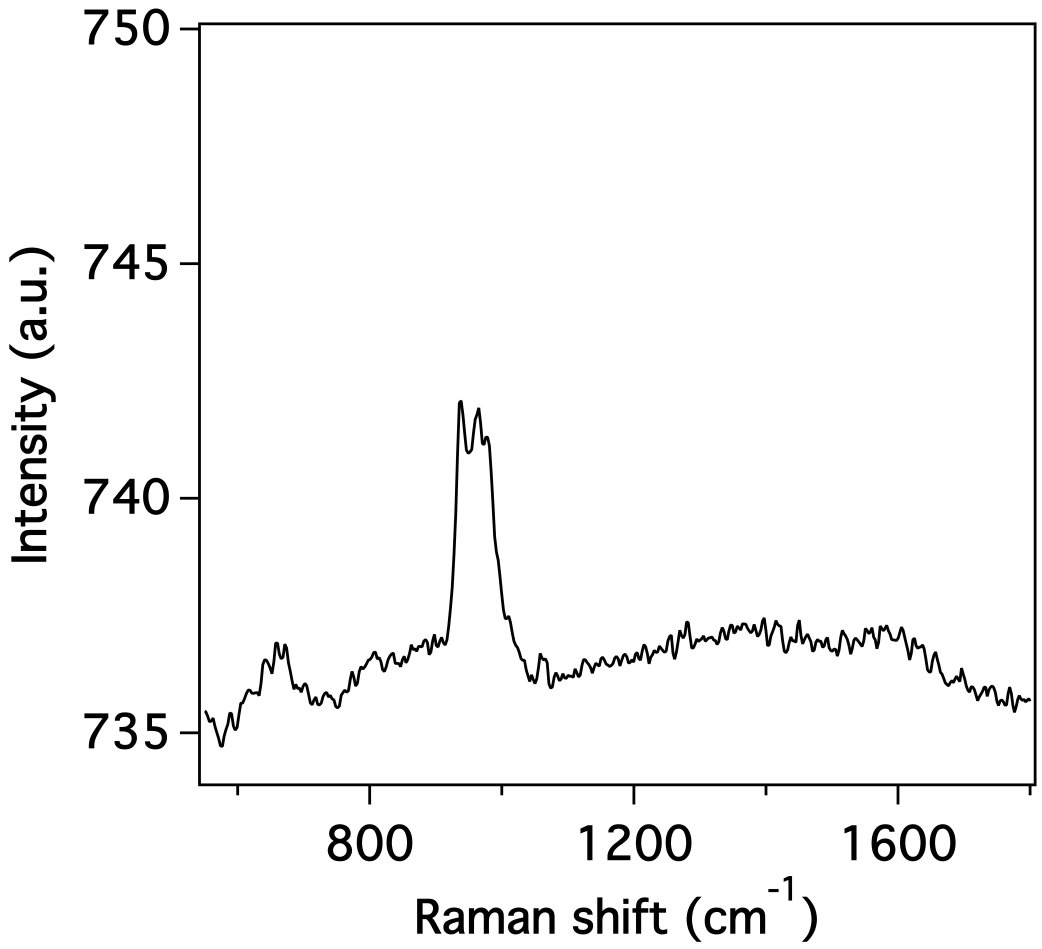

Figure S6. SERS spectrum (spatially-averaged) of PAO1C grown in FAB + glucose for 24 h.

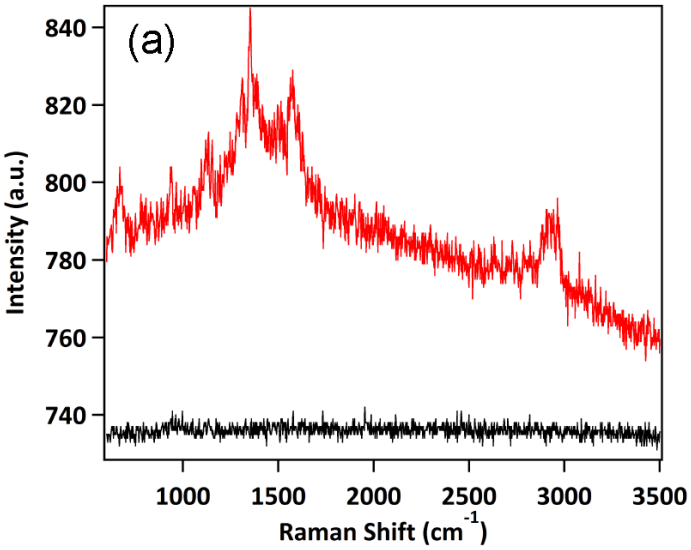
(a)
Intensity (a.u.)
840
820
800
780
760
740
1000
1500
2000
2500
3000
3500
Raman Shift (cm-1)

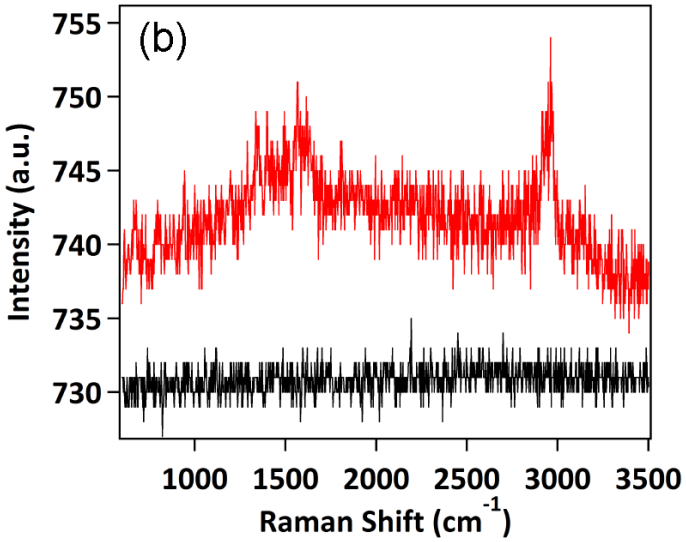
(b)
Intensity (a.u.)
755
750
745
740
735
730
1000
1500
2000
2500
3000
3500
Raman Shift (cm-1)

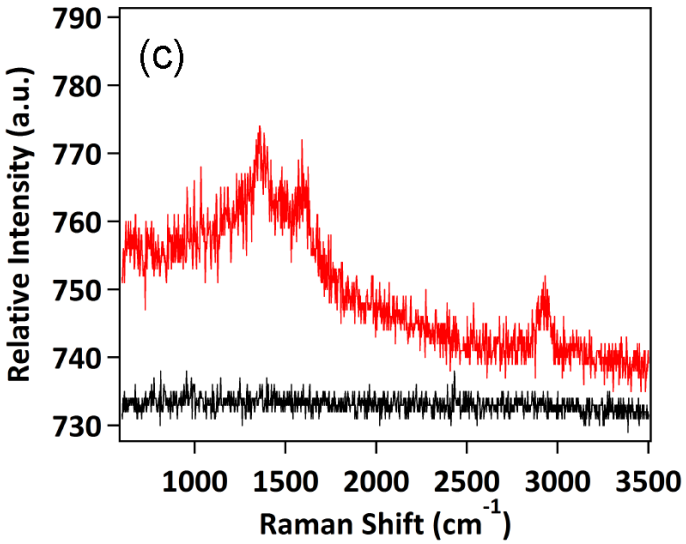
(c)
Relative Intensity (a.u.)
790
780
770
760
750
740
730
1000
1500
2000
2500
3000
3500
Raman Shift (cm-1)

Figure S7. Single point SERS spectra from regions of high (red) and low (black) SERS intensity from Raman images collected from pellicle biofilms derived from *P. aeruginosa*. (a) FRD1 grown on glucose; (b) FRD1 grown on glutamate; (c) PAO1C grown on glutamate.

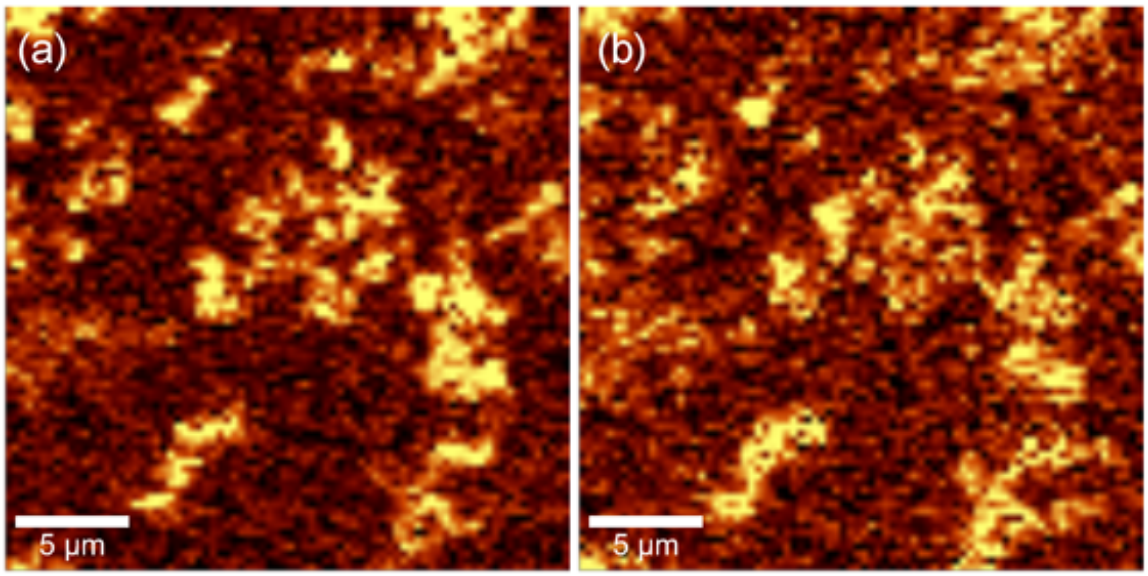

Figure S8. Comparison of Raman images of a region of a pellicle biofilm grown from glutamate. (a) Raman image integrated over 600-1800 cm^{-1}. (b) Raman image integrated from 2800-3000 cm^{-1}.

SERS spectra of washed planktonic cells of *Pseudomonas aeruginosa* are essentially identical to previously published normal Raman spectra of planktonic *Pseudomonas*. See Masyuko, R., *et al.*, *Analyst* **2014**, 139, 5700-5708.